Visualization of the Conventional Outflow Pathway in the Living Human Eye

Larry Kagemann, PhD,[1,2] Gadi Wollstein, MD,[1] Hiroshi Ishikawa, MD,[1,2] Zachary Nadler, BS,[1] Ian A. Sigal, PhD,[1,2,3] Lindsey S. Folio, BS,[1] Joel S. Schuman, MD[1,2,3]

Purpose: We sought to visualize the aqueous outflow system in 3 dimensions (3D) in living human eyes, and to investigate the use of commercially available spectral-domain optical coherence tomographic (SD-OCT) systems for this purpose.

Design: Prospective, observational study.

Participants: One randomly determined eye in each of 6 normal healthy subjects was included.

Testing: We performed 3D SD-OCT imaging of the aqueous humor outflow structures with 2 devices: The Cirrus HD-OCT and the Bioptigen SDOIS.

Main Outcome Measures: We created 3D virtual castings of Schlemm's canal (SC) and more distal outflow structures from scan data from each device.

Results: Virtual casting of the SC provided visualization of more aqueous vessels branching from SC than could be located by interrogating the 2-dimensional (2D) image stack. Similarly, virtual casting of distal structures allowed visualization of large and small aqueous outflow channel networks that could not be appreciated with conventional 2D visualization.

Conclusions: The outflow pathways from SC to the superficial vasculature can be identified and tracked in living human eyes using commercially available SD-OCT.

Financial Disclosure(s): Proprietary or commercial disclosure may be found after the references.
Ophthalmology 2012;119:1563–1568

Glaucoma is the second leading cause of blindness worldwide,[1] and the most important risk factor for glaucoma is elevated intraocular pressure (IOP).[2,3] The IOP is regulated by a balance between the production and outflow of aqueous humor. The conventional aqueous humor outflow pathway consists of passage through the trabecular meshwork draining into Schlemm's canal (SC) and then to aqueous veins.[4] Aqueous veins may carry aqueous humor directly to scleral veins or intervening vascular plexuses, all of which eventually empty into scleral veins.[4,5] Despite the importance of this basic physiologic function, it occurs outside the view of the clinician.

We previously demonstrated the ability to visualize SC noninvasively in living human eyes in 2 dimensions (2D), and more distal structures in a cadaver eye outflow model in 3 dimensions (3D).[6,7] Those images were acquired with a spectral domain-optical coherence tomography (SD-OCT) device in an experimental configuration. The purpose of this study was to enable 3D visualization of the aqueous outflow system in living human eyes using commercially available SD-OCT systems.

Methods

The study was conducted in accordance to the tenets of the declaration of Helsinki and the Health Insurance Portability and Accountability Act. The institutional review board of the University of Pittsburgh approved the study. All subjects gave written informed consent before participation in the study.

Imaging of SC in Human Eyes

Six healthy volunteers were recruited from the staff and faculty of the University of Pittsburgh Medical Center Eye Center. Schlemm's canal and aqueous veins were imaged using 2 commercially available SD-OCT devices: The Cirrus HD-OCT (Carl Zeiss Meditec, Dublin, CA) and a modified Bioptigen SDOIS (Bioptigen, Research Triangle Park, NC). The Cirrus light source has a 50-nm bandwidth centered at 840 nm, resulting in a 5-μm coherence length in tissue. The Bioptigen optics engine was coupled with a quad diode light source with an 870-nm center wavelength and a 200-nm bandwidth (Q870, Superlum Ltd, Dublin, Ireland). The light source had a coherence length of 1.3 μm in tissue.

Two scan protocols were used; one optimized for the acquisition of 3D data (the "volume" protocol, 512×512 A-scans with no averaging; ~9.4-second acquisition time) and one optimized for visualization of individual frames (the "2D slice" protocol, 700×40 A-scans, each averaged 8 times at acquisition; ~8-second acquisition time). Each protocol imaged a 4×4-mm transverse area of the limbus with a 2-mm A-scan length at the 3, 6, and 12 o'clock positions. Sequential scans in the volume protocol had a center-to-center spacing of 7.8 μm. With a lateral resolution of 20 μm, there was a high level of overlap (resampling) of tissue with any single point within the scan volume being sampled by 5 axial scans (center plus nearest neighbors in the x–y plane). Sequential scans in the 2D slice protocol were separated by 100 μm. All scans were oriented so that the scan cube was tangential to the limbus and the center scan was radial to the limbus.

The commercially available Cirrus HD-OCT had 2 Food and Drug Administration–approved anterior segment scan protocols. The 512×128 A-scan "cube" protocol (~2.5-second scan time)

ISSN 0161-6420/12/$–see front matter
doi:10.1016/j.ophtha.2012.02.032

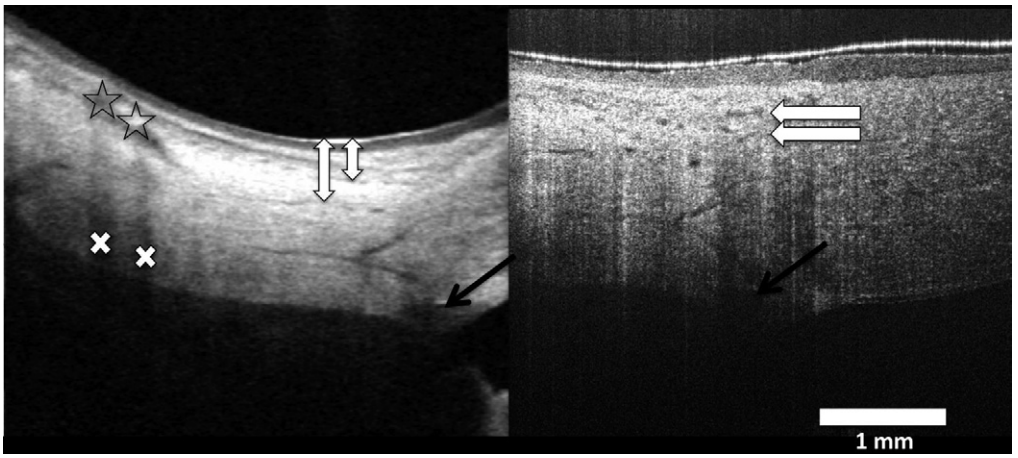

Figure 1. The Cirrus image of the limbus (left) clearly reveals Schlemm's canal (black arrows), as well as a distinctive "fallen Y" aqueous vein. The characteristics of this structure can be used to locate the same cross-sectional image within the Bioptigen image data (right). Two distinct layers of aqueous venous plexuses are visible (white block arrows, right), at 2 depths within the limbus (white block arrows, left). Unlike blood vessels (stars), which cast vertical shadows into the scan (Xs), aqueous veins do not create shadowing artifacts in the image (white bar = 1 mm).

Table 1. Aqueous Venous Plexus Characteristics

Location	Mean (SD) Distance from Surface to Aqueous Venous Plexus (μm)	Mean (SD) Aqueous Vein Diameter (μm)
Nasal superficial	133.17 (23.29)	38.28 (7.22)
Inferior superficial	95.94 (12.44)	33.03 (8.72)
Temporal superficial	115.30 (14.08)	32.88 (9.23)
Superior superficial	99.50 (52.71)	18.07 (8.58)
Nasal deep	295.61 (59.72)	48.53 (9.05)
Inferior deep	318.35 (68.81)	74.42 (20.56)
Temporal deep	258.58 (51.77)	39.46 (6.13)
Superior deep	270.55 (132.67)	34.22 (16.49)

SD = standard deviation.
The distance between the surface of the limbus and each of the 2 layers of aqueous venous plexuses was measured in each quadrant. The diameter of aqueous veins within those plexuses was also measured.

was used, covering a 4×4-mm area of the limbus at 3, 6, and 12 o'clock. Unlikethe Bioptigen, which was capable of orienting the B-scans at any arbitrary angle, only the 3 and 6 o'clock Cirrus B-scans had a radial orientation relative to the limbus; the 12 o'clock scan had a tangential orientation. Sequential frames in the Cirrus scans had a 31-μm center-to-center separation. Raw OCT signal data were exported from both devices.

Image Processing

Scans were preprocessed with a custom-written OCT browser of our own design,[8–10] and then visualized in 3D using ImageJ Fiji (ImageJ 1.45k java; available at: http://rsb.info.nih.gov/ij/). Cirrus scans were preprocessed with a 3×3×3 averaging kernel. Specifically, each voxel in the dataset was replaced by the average of 27 voxels in surrounding 3×3×3, 3D space. Bioptigen volume images were preprocessed with a flat 5×5 averaging kernel. Each voxel was replaced with the average of the surrounding 5×5-voxel, 2D plane. Averaging protocols were selected subjectively based on the appearance of the outcome. Processing time for

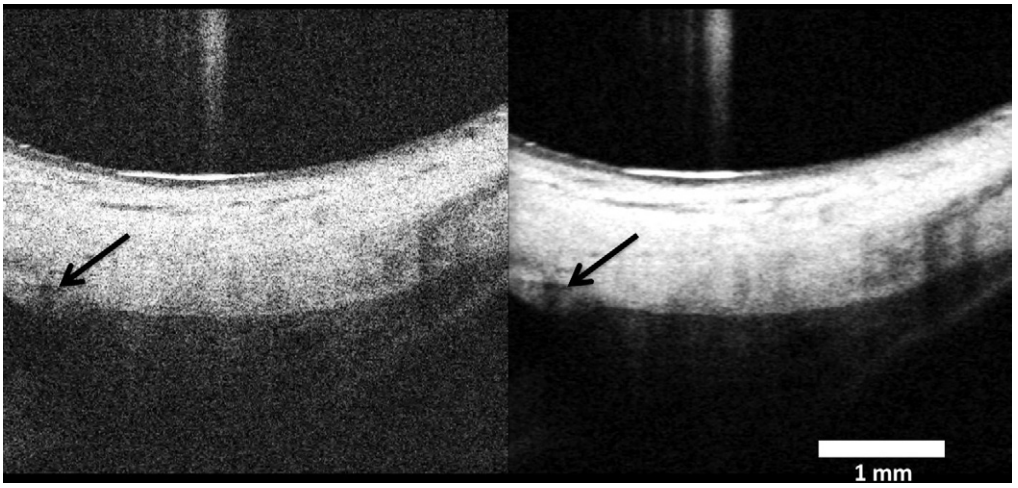

Figure 2. Averaging of raw Cirrus scan data removes speckle noise (left), clearly revealing Schlemm's canal (black, arrow) and other outflow structures (white bar = 1 mm).

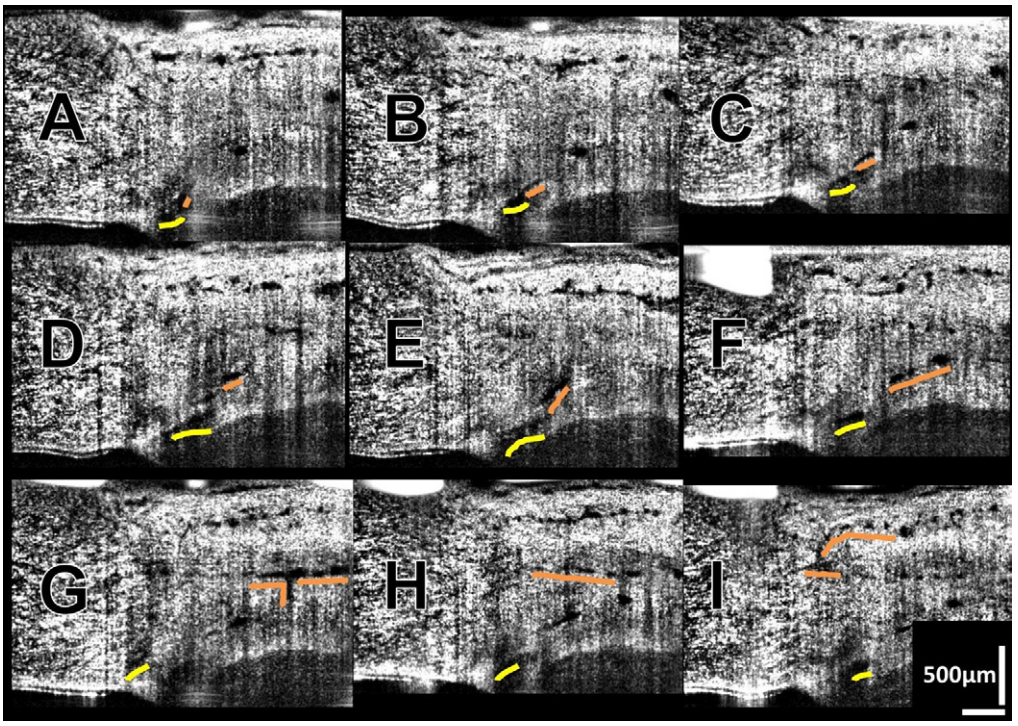

Figure 3. Contrast-enhanced image sequence obtained with the Bioptigen; the pathway (underlined in orange) from Schlemm's canal (underlined in yellow) is traced to the midlimbal intrascleral plexus. These images are from a sequence of 40 axial slices of the limbus acquired in 8 seconds. The center-to-center spacing of these slices is 100 μm.

averaging was approximately 1 minute per image for both Bioptigen and Cirrus.

The Fiji "enhance local contrast" filter was used to improve visualization of structure throughout. To create virtual castings, images were inverted so that the black collector channels appeared as white structures. The "subtract background" filter was applied with a 30-pixel kernel. Images were resampled to provide a 1:1:1 voxel aspect ratio in 3D. Contrast was adjusted to isolate the collector channels and the volumes rendered using the 3D viewer plugin. The total time to produce a 3D visualization was approximately 20 minutes, although multiple attempts to maximize visualization of structures were common. Varying levels of noise sources surrounding structures of interest necessitated flexibility in the degree to which noise was suppressed, to minimize noise content with minimal loss of image content.

Two distinct layers of aqueous venous plexuses were subjectively identified in the 2D visualizations (Fig 1, white block arrows). The distance from the surface of the limbus to each aqueous venous plexus was measured in the 2D slices in nasal, inferior, temporal, and superior quadrants. The diameters of aqueous veins in each layer of the aqueous venous plexus were

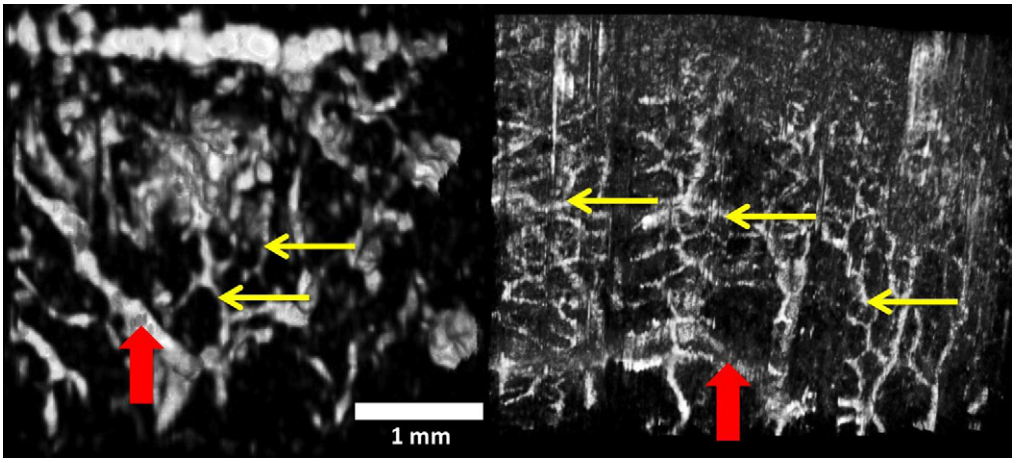

Figure 4. Inclusion of more noise (right, Bioptigen) allows a more complete virtual casting of the aqueous humor outflow pathway (yellow arrows), compared with a casting with heavily suppressed noise (left, Cirrus), which washes out many of the outflow structures (yellow arrows) leaving, for the most part, large blood vessels (red arrows; white bar = 1 mm).

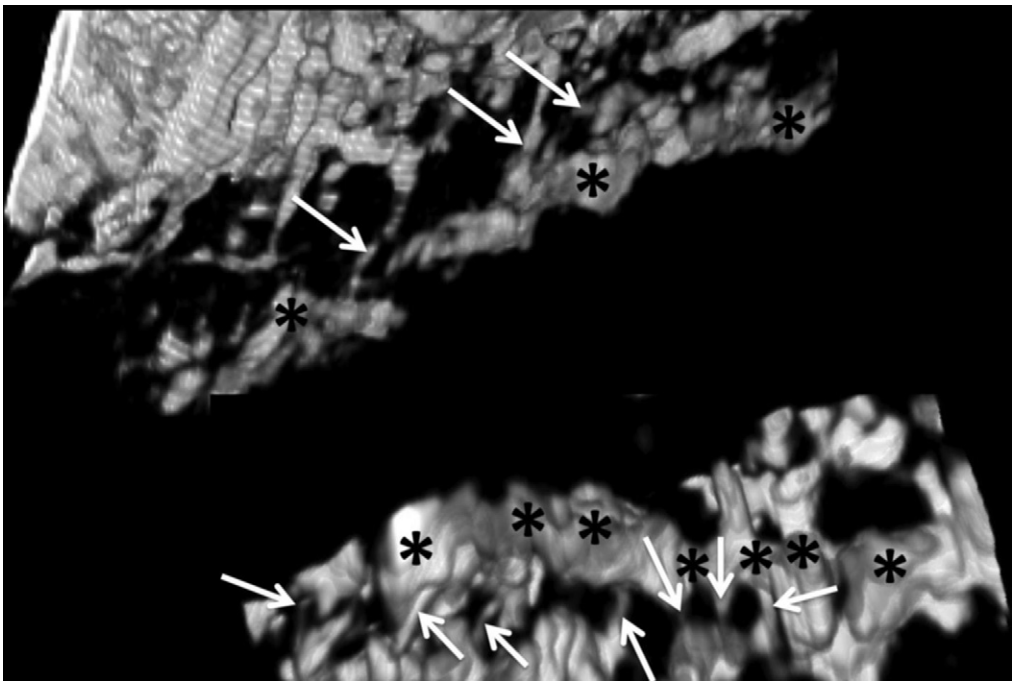

Figure 5. Two virtual castings of Schlemm's canal were produced from volumetric anterior segment scans of the limbus obtained with the Cirrus device. Schlemm's canal is marked with asterisks, and locations of connecting collector channels at ostia are marked with arrows.

measured in each quadrant. No fewer than 6 of the 40 frames of the "2D" scan protocol were included for each location when venous plexus depth and aqueous vein diameter were assessed.

Results

Four men and 2 women (average age, 38.5 and 29 years, respectively) were imaged on 2 different days. Outflow pathways were readily visible in both Cirrus and Bioptigen images from all eyes (Fig 1). The 2D slices reveal both outflow and vascular structures. Blood vessels cast vertical shadows in OCT images[11] (Fig 1, *x*s). Shadows can be used to identify blood vessels (Fig 1, stars). Aqueous veins can be identified by tracing their pathway to SC, and their identity as aqueous veins is confirmed by the lack of shadows (Fig 1, block arrows). The average depth of the superficial and deep aqueous venous plexuses and the average aqueous vein diameters are presented in Table 1. Acquisition of 3D volumetric samples enabled identification of the same location within the limbus in both scan sets, based on subjective observation of outflow pathway morphology (Fig 1). Speckle noise obscured visualization of SC and aqueous veins within the raw Cirrus scans, but 3×3×3 averaging reduced speckle and allowed clear visualization (Fig 2). Utilizing adjacent frames, the pathway from SC to the midlimbal intrascleral plexus could be traced (Fig 3).

Virtual casting of the aqueous humor outflow structures between SC and the episcleral vasculature, as well as surrounding blood vessels, whose identity is suggested by their relatively large size, was feasible with the data produced on each system (Fig 4). The degree to which noise was suppressed altered the image content. Leaving more noise (Fig 4, left, Bioptigen casting) allowed visualization of aqueous outflow microvasculature with a "fishnet" appearance. Removal of more noise (Fig 4, right, Cirrus casting) eliminated visualization of the aqueous humor microvasculature, leaving only large blood vessels in the casting.

Figure 5 presents the first virtual castings of SC (asterisks) in the living human eye. Several collector channels (arrows) and aqueous veins extending from SC were observed within the 4-mm section of SC. When the 2D image stack that produced these castings was reviewed, the presence of 4 aqueous vein branch points was not evident. The SC could be cast from all Cirrus scans at both nasal and temporal quadrants (Fig 6, SC, asterisks). When the castings were rotated in 3D space, collector channels emanating from SC could be observed in 9 of the 12 castings.

Discussion

In this study, we have demonstrated the ability of SD-OCT to acquire volumetric scans of the limbus, from which the outflow pathway can be tracked from SC to the superficial vascular plexuses in 2D image sequences and from which virtual castings of those same outflow structures can be produced. We also found that averaging the raw scan data improved visualization of the outflow pathway. We present the first 3D castings of outflow structures in the living human eye.

The ability to visualize SC and surrounding aqueous veins in 3D increases the ability to detect detailed information of the outflow pathway, such as the branch points, in comparison with the 2D images. We have previously described a number of instances in which 3D visualization of a structure within a raster scan set reveals its identity.[12] In this study, the observation of small vessels adjacent to and emanating from SC allowed their identification as collector

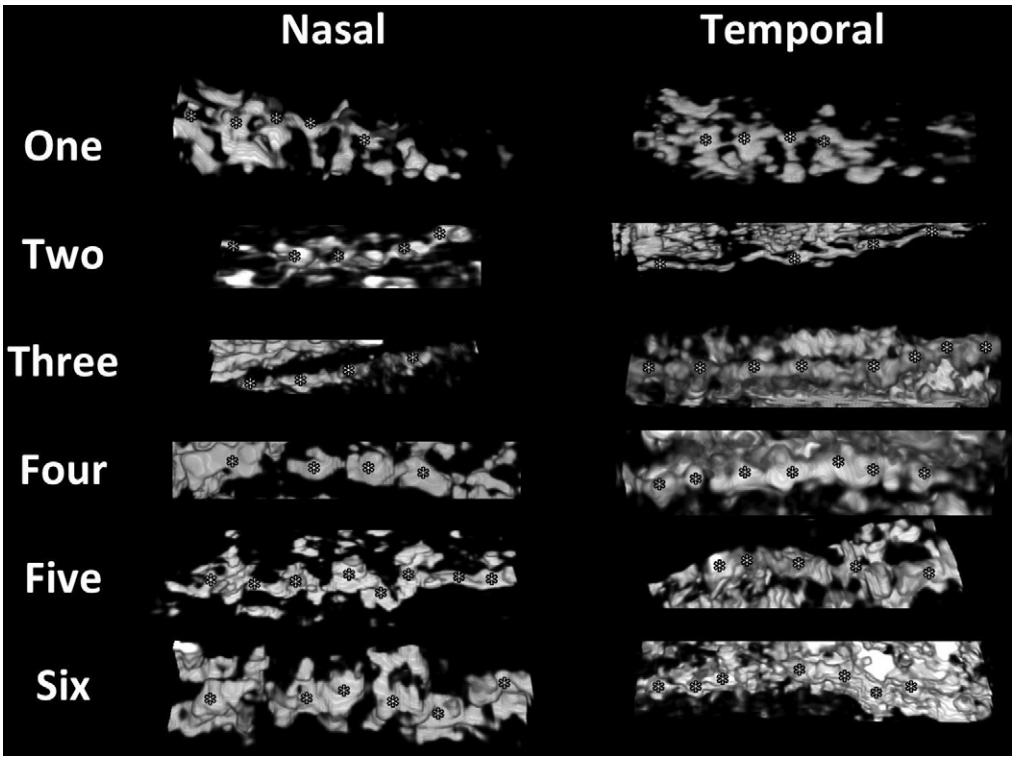

Figure 6. Schlemm's canal (*) was virtually cast in all nasal and temporal quadrants. Visibility of collector channels varied with noise suppression.

channels despite their weak and hidden appearance when observed in 2D.

The ability to cast SC in 3D could improve the management and treatment of glaucoma. Visualization of SC and collector channels could give guidance to the glaucoma surgeon wishing to improve aqueous outflow through the conventional pathways. The trabecular meshwork and inner wall of SC could be removed specifically in the region of collector channels and their ostia as well as aqueous veins to maximize the impact of that surgery on outflow facility and reduction of IOP. The same is true for devices that would reside in SC and bypass the trabecular meshwork and inner wall of SC—placement at the sites in proximity of collector channel ostia would potentially maximize their effectiveness in IOP reduction because aqueous would not have to traverse long distances in SC before exiting through the collector channels. Conversely, it is possible that leaving currently active regions of aqueous humor outflow undisturbed and using implanted devices to enhance outflow by positioning them in regions devoid of observable aqueous vein/SC branch points would maximize outflow. This casting technique may be useful in elucidating the optimal implant placement strategy. This hypothesis could be tested in the perfused cadaver eye model.

The findings in the present study also include the first virtual castings of the distal outflow vasculature in a living eye, similar to the castings of cadaver eyes published in a previous study.[7] Unlike the previous study, the casting in the living eye includes patent blood vessels (Fig 1). It is likely that, based on their relative size, the large vessels more prominent in the Cirrus casting in Fig 4 are blood vessels. The small aqueous humor vessels visible in the Bioptigen casting in Fig 4 feature a distinct network of straight segments sharing branch points. Some evidence of this same microvasculature exists in the Cirrus casting, but the extent to which it pervades the morphology of the aqueous humor outflow vasculature cannot be appreciated. Unfortunately, visualization of the smaller vessels cannot be accomplished without the inclusion of substantial image noise. A study focusing on the morphology of small aqueous vessels is currently underway.

In conclusion, 3D virtual casting of the aqueous outflow vasculature is possible in living human eyes with existing, off-the-shelf, general-purpose SD-OCT technology. The outflow pathways from SC to the superficial vasculature can be identified and tracked, and SC can be cast in 3D from these scans. Postprocessing is required to maximize the visualization of the content within.

References

1. Quigley HA, Broman AT. The number of people with glaucoma worldwide in 2010 and 2020. Br J Ophthalmol 2006; 90:262–7.
2. Sommer A, Tielsch JM, Katz J, et al, Baltimore Eye Survey Research Group. Relationship between intraocular pressure and primary open angle glaucoma among white and black Americans: the Baltimore Eye Survey. Arch Ophthalmol 1991;109:1090–5.

3. Haefliger IO. Risk factors associated with glaucoma [in French]. Klin Monbl Augenheilkd 1997;210:265–8.
4. van der Merwe EL, Kidson SH. Advances in imaging the blood and aqueous vessels of the ocular limbus. Exp Eye Res 2010;91:118–26.
5. Grant WM. Clinical measurements of aqueous outflow. Am J Ophthalmol 1951;34:1603–5.
6. Kagemann L, Wollstein G, Ishikawa H, et al. Identification and assessment of Schlemm's canal by spectral-domain optical coherence tomography. Invest Ophthalmol Vis Sci 2010; 51:4054–9.
7. Kagemann L, Wollstein G, Ishikawa H, et al. 3D visualization of aqueous humor outflow structures in-situ in humans. Exp Eye Res 2011;93:308–15.
8. Ishikawa H, Gurses-Ozden R, Hoh ST, et al. Grayscale and proportion-corrected optical coherence tomography images. Ophthalmic Surg Lasers 2000;31:223–8.
9. Ishikawa H, Piette S, Liebmann JM, Ritch R. Detecting the inner and outer borders of the retinal nerve fiber layer using optical coherence tomography. Graefes Arch Clin Exp Ophthalmol 2002;240:362–71.
10. Ishikawa H, Stein DM, Wollstein G, et al. Macular segmentation with optical coherence tomography. Invest Ophthalmol Vis Sci 2005;46:2012–7.
11. Girard MJ, Strouthidis NG, Ethier CR, Mari JM. Shadow removal and contrast enhancement in optical coherence tomography images of the human optic nerve head. Invest Ophthalmol Vis Sci 2011;52:7738–48.
12. Kagemann L, Ishikawa H, Wollstein G, et al. Visualization of 3-D high speed ultrahigh resolution optical coherence tomographic data identifies structures visible in 2D frames. Opt Express [serial online] 2009;17:4208-20. Available at: http://www.opticsinfobase.org/abstract.cfm?URI=oe-17-5-4208. Accessed January 21, 2012.

Footnotes and Financial Disclosures

Originally received: October 10, 2011.
Final revision: February 16, 2012.
Accepted: February 17, 2012.
Available online: June 8, 2012. Manuscript no. 2011-1487.

[1] Department of Ophthalmology, UPMC Eye Center, Eye and Ear Institute, Ophthalmology and Visual Science Research Center, University of Pittsburgh School of Medicine, Pittsburgh, Pennsylvania.

[2] Department of Bioengineering, Swanson School of Engineering, University of Pittsburgh, Pittsburgh, Pennsylvania.

[3] The McGowan Institute for Regenerative Medicine, University of Pittsburgh School of Medicine, Pittsburgh, Pennsylvania.

Financial Disclosure(s):
The authors have made the following disclosures: Joel S. Schuman – Royalties – Intellectual property licensed by Massachusetts Institute of Technology and Massachusetts Eye and Ear Infirmary to Carl Zeiss Meditec, Inc.

Supported in part by National Institute of Health contracts R01-EY13178, and P30-EY08098 (Bethesda, MD), The Eye and Ear Foundation (Pittsburgh, PA), unrestricted grants from Research to Prevent Blindness (New York, NY) and the American Health Assistance Foundation.

Correspondence:
Joel S. Schuman, MD, UPMC Eye Center, Department of Ophthalmology, University of Pittsburgh School of Medicine, 203 Lothrop Street, Eye and Ear Institute, Suite 816, Pittsburgh, PA. E-mail: SchumanJS@upmc.edu